CP asymmetries of $\bar{B} \to X_s/X_d\gamma$ in models with three Higgs doublets

A. G. Akeroyd,[1,*] Stefano Moretti,[1,†] Tetsuo Shindou,[2,‡] and Muyuan Song[1,§]

[1]*School of Physics and Astronomy, University of Southampton, Highfield, Southampton SO17 1BJ, United Kingdom*

[2]*Division of Liberal-Arts, Kogakuin University, 2665-1 Nakano-machi, Hachioji, Tokyo 192-0015, Japan*

(Received 18 September 2020; accepted 11 January 2021; published 29 January 2021)

Direct *CP* asymmetries ($\mathcal{A}_{CP}$) in the inclusive decays of $\bar{B} \to X_s\gamma$ and $\bar{B} \to X_{s+d}\gamma$ of the order of 1% will be probed at the BELLE II experiment. In this work, three such asymmetries are studied in the context of a three-Higgs-doublet model (3HDM), and it is shown that all three $\mathcal{A}_{CP}$ can be as large as the current experimental limits. Of particular interest is the $\mathcal{A}_{CP}$ for $\bar{B} \to X_{s+d}\gamma$, which is predicted to be effectively zero in the Standard Model (SM). A measurement of 2.5% or more for this observable with the full BELLE II data would give 5σ evidence for physics beyond the SM. We display parameter space in the 3HDM for which such a clear signal is possible.

DOI: 10.1103/PhysRevD.103.015035

I. INTRODUCTION

A new particle with a mass of around 125 GeV was discovered by the ATLAS and CMS collaborations of the Large Hadron Collider (LHC) [1,2]. At present, the measurements of its properties are in very good agreement (within experimental error) with those of the Higgs boson of the Standard Model (SM), and hence the simplest interpretation is that the 125 GeV scalar boson is the (lone) Higgs boson of the SM (h). However, an alternative possibility is that it is the first scalar to be discovered from a nonminimal Higgs sector, which contains additional scalar isospin doublets or higher representations (e.g., scalar isospin triplets). This scenario will be probed by more precise future measurements of its branching ratios (BRs), which might eventually show deviations from those of the SM Higgs boson. There could also be the possibility of discovering additional electrically neutral scalars (H or A) and/or electrically charged scalars ($H^\pm$), and such searches form an active part of the LHC experimental program. In the context of a two-Higgs-doublet model (2HDM) the lack of direct observation of an $H^\pm$ at the LHC together with precise measurements of SM processes exclude parameter space of $\tan\beta$ (which is present in the Yukawa couplings) and $m_{H^\pm}$ (mass of the $H^\pm$), where $\tan\beta = v_2/v_1$ and v_1 and v_2 are the vacuum expectation values (VEVs) of the two Higgs doublets, respectively (for reviews see, e.g., [3,4]).

In a three-Higgs-doublet model (3HDM) the Yukawa couplings of the two charged scalars depend on the four free parameters ($\tan\beta$, $\tan\gamma$, θ, and δ) of a unitary matrix that rotates the charged scalar fields in the weak eigenbasis to the physical charged scalar fields [5]. The phenomenology of the lightest $H^\pm$ in a 3HDM [6–8] can be different to that of the $H^\pm$ in a 2HDM due to the larger number of parameters that determine its fermionic couplings.

The decay $b \to s\gamma$, whose BR has been measured to be in good agreement with that of the SM, provides strong constraints on the parameter space of charged scalars in 2HDMs and 3HDMs. In the well-studied 2HDM type II the bound $m_{H^\pm} > 480$ GeV [9] can be obtained and is valid for all $\tan\beta$. More precise measurements of $\mathrm{BR}(b \to s\gamma)$ at the ongoing BELLE II experiment will sharpen these constraints, but it is very unlikely that measurements of $\mathrm{BR}(b \to s\gamma)$ alone could provide evidence for the existence of an $H^\pm$. However, the direct *CP* asymmetry in $b \to s\gamma$ will be probed at the 1% level, and can be enhanced significantly above the SM prediction by additional complex phases that are present in models of physics beyond the SM [10]. In the context of 3HDMs we study the magnitude of three different direct *CP* asymmetries that involve $b \to s\gamma$, including the contribution of both charged scalars for the first time. We display parameter space in 3HDMs that would give a clear signal for these three observables at the BELLE II experiment.

This work is organized as follows. In Sec. II the measurements of $b \to s\gamma$ are summarized and the *CP* asymmetries in this decay are described. In Sec. III the

*a.g.akeroyd@soton.ac.uk
†S.Moretti@soton.ac.uk
‡shindou@cc.kogakuin.ac.uk
§ms32g13@soton.ac.uk

contribution of the charged scalars in a 3HDM to the partial decay width of $b \to s(d)\gamma$ is presented. Section IV contains our results, and conclusions are given in Sec. V.

II. DIRECT *CP* ASYMMETRIES IN $\bar{B} \to X_s\gamma$ AND $\bar{B} \to X_{s+d}\gamma$

In this section the experimental measurements of the inclusive decays $\bar{B} \to X_s\gamma$ and $\bar{B} \to X_{s+d}\gamma$ (charged conjugated processes are implied) are described, followed by a discussion of direct *CP* asymmetries in these decays. The symbol B signifies B^+ or B^0 (which contain anti-b quarks) while $\bar{B}$ signifies B^- or $\overline{B^0}$ (which contain b quarks). The symbol X_s denotes any hadronic final state that originates from a strange quark hadronizing (e.g., states with at least one kaon), X_d means any hadronic final state that originates from a down quark hadronizing (e.g., states with at least one pion), and X_{s+d} denotes any hadronic final state that is X_s or X_d.

A. Experimental measurements of $\bar{B} \to X_s\gamma$ and $\bar{B} \to X_{s+d}\gamma$

There are two ways to measure the BR of the inclusive decays $\bar{B} \to X_{s/d}\gamma$:

(i) The fully inclusive method;
(ii) The sum-of-exclusives method (also known as "semi-inclusive").

In the fully inclusive approach, only a photon from the signal $\bar{B}$ (or B) meson in the $B\bar{B}$ event, which decays via $b \to s/d\gamma$, is selected. Consequently, this method cannot distinguish between hadronic states X_s and X_d, and what is measured is actually the sum of $\bar{B} \to X_s\gamma$ and $\bar{B} \to X_d\gamma$. From the other $\bar{B}$ (or B) meson ("tag B meson") either a lepton (e or μ) can be selected or full reconstruction (either hadronic or semileptonic) can be carried out. The former method has a higher signal efficiency, but the latter method has greater background suppression. Measurements of $\bar{B} \to X_{s+d}\gamma$ using the fully inclusive method with leptonic tagging have been carried out by the CLEO collaboration [11], the *BABAR* collaboration [12], and the BELLE collaboration [13]. A measurement of $\bar{B} \to X_{s+d}\gamma$ using the fully inclusive method with full (hadronic) reconstruction of the tag $\bar{B}$ meson has so far only been carried out by the *BABAR* collaboration [14]. At the current integrated luminosities (0.5 to 1 ab^{-1}) the errors associated with measurements that involve full reconstruction are significantly larger than the errors from measurements with leptonic tagging. However, with the larger integrated luminosity at BELLE II (50 ab^{-1}) it is expected that both approaches will provide roughly similar errors. To obtain a measurement of $\bar{B} \to X_s\gamma$ alone, the contribution of $\bar{B} \to X_d\gamma$ (which is smaller by roughly $|V_{td}/V_{ts}|^2 \approx 1/20$ in the SM, which has also been confirmed experimentally) is subtracted.

In the sum-of-exclusives approach the selection criteria are sensitive to as many exclusive decays as possible in the hadronic final states X_s and X_d of the signal $\bar{B}$, as well as requiring a photon from $b \to s/d\gamma$. In contrast to the fully inclusive approach, no selection is made on the other B meson in the $B\bar{B}$ event. The sum-of-exclusives method is sensitive to which decay, $b \to s\gamma$ or $b \to d\gamma$, occurred and so this approach measures $\bar{B} \to X_s\gamma$ or $\bar{B} \to X_d\gamma$. It has different systematic uncertainties to that of the fully inclusive approach. Measurements of $\bar{B} \to X_s\gamma$ have been carried out by the *BABAR* collaboration [15] and the BELLE collaboration [16]. Currently, 38 exclusive decays in $\bar{B} \to X_s\gamma$ (about 70% of the total BR) and 7 exclusive decays in $\bar{B} \to X_d\gamma$ [17] are included. At current integrated luminosities, the error in the measurement of $\bar{B} \to X_s\gamma$ is about twice that of the fully inclusive approach, whereas at BELLE II integrated luminosities the latter is still expected to give the more precise measurement.

Measurements in both of the above approaches are made with a lower cutoff on the photon energy E_γ in the range 1.7–2.0 GeV, and then an extrapolation is made to $E_\gamma > 1.6$ GeV using theoretical models. The current world average for the above six measurements of $\bar{B} \to X_s\gamma$ is [18]

$$\mathcal{B}_{s\gamma}^{\rm exp} = (3.32 \pm 0.15) \times 10^{-4} \quad \text{with} \quad E_\gamma > 1.6\,\text{GeV}. \tag{1}$$

The error is currently 4.5% and is expected to be reduced to around 2.6% with the final integrated luminosity at the BELLE II experiment [19].

The theoretical prediction including corrections to order α_s^2 [i.e., next-to-next-to-leading order (NNLO)] is [20]

$$\mathcal{B}_{s\gamma}^{\rm SM} = (3.40 \pm 0.17) \times 10^{-4} \quad \text{with} \quad E_\gamma > 1.6\ \text{GeV}.$$

There is excellent agreement between the world average and the NNLO prediction in the SM. Consequently, $\mathcal{B}_{s\gamma}^{\rm exp}$ allows stringent lower limits to be derived on the mass of new particles, most notably the mass of the charged scalar ($m_{H^\pm} > 480$ GeV [9], as mentioned earlier) in the 2HDM (type II).

B. Direct *CP* asymmetries of $\bar{B} \to X_s\gamma$ and $\bar{B} \to X_{s+d}\gamma$

Although it is clear that measurements of $\text{BR}(\bar{B} \to X_s\gamma)$ alone will not provide evidence for new physics with BELLE II data, the direct *CP* asymmetry in this decay might [10]. Direct *CP* asymmetries in $\bar{B} \to X_s\gamma$ and $\bar{B} \to X_d\gamma$ are defined as follows:

$$\mathcal{A}_{X_{s(d)}\gamma} = \frac{\Gamma(\bar{B} \to X_{s(d)}\gamma) - \Gamma(B \to X_{\bar{s}(\bar{d})}\gamma)}{\Gamma(\bar{B} \to X_{s(d)}\gamma) + \Gamma(B \to X_{\bar{s}(\bar{d})}\gamma)}. \tag{2}$$

If B is B^+ (and so $\bar{B} = B^-$) in the definition of $\mathcal{A}_{X_{s(d)}\gamma}$ then the *CP* asymmetry is for the charged B mesons, is labelled

as $\mathcal{A}^{\pm}_{X_s\gamma}$ or $\mathcal{A}^{\pm}_{X_d\gamma}$, and can be individually probed in a search that reconstructs X_s or X_d (the sum-of-exclusives method). If B is B^0 the CP asymmetry is for the neutral B mesons, is labelled as $\mathcal{A}^0_{X_s\gamma}$ or $\mathcal{A}^0_{X_d\gamma}$, and can also be individually probed. A general formula for the short-distance contribution (from "direct photons") to $\mathcal{A}_{X_{s(d)}\gamma}$ in terms of Wilson coefficients was derived in Ref. [10]. Prior to the publication of Ref. [10] a few works [21–23] had calculated $\mathcal{A}_{X_s\gamma}$ in the SM and in specific extensions of it that include a charged Higgs boson. The formula for $\mathcal{A}_{X_{s(d)}\gamma}$ in Ref. [10] was the first complete calculation of the asymmetry in terms of all of the contributing Wilson coefficients, and was extended 12 years later to include the long-distance contributions (from "resolved photons") in Ref. [24]. In approximate form $\mathcal{A}_{X_{s(d)}\gamma}$ is as follows:

$$\begin{aligned}\mathcal{A}_{X_{s(d)}\gamma} \approx \pi\Bigg\{&\left[\left(\frac{40}{81}-\frac{40}{9}\frac{\Lambda_c}{m_b}\right)\frac{\alpha_s}{\pi}+\frac{\tilde{\Lambda}^c_{17}}{m_b}\right]\mathrm{Im}\frac{C_2}{C_{7\gamma}}\\ &-\left(\frac{4\alpha_s}{9\pi}-4\pi\alpha_s e_{\mathrm{spec}}\frac{\tilde{\Lambda}_{78}}{m_b}\right)\mathrm{Im}\frac{C_{8g}}{C_{7\gamma}}\\ &-\left(\frac{\tilde{\Lambda}^u_{17}-\tilde{\Lambda}^c_{17}}{m_b}+\frac{40}{9}\frac{\Lambda_c}{m_b}\frac{\alpha_s}{\pi}\right)\mathrm{Im}\left(\epsilon_{s(d)}\frac{C_2}{C_{7\gamma}}\right)\Bigg\}.\end{aligned} \tag{3}$$

The above four asymmetries are obtained from Eq. (3) with the choices for e_{spec} (the charge of the spectator quark) and $\epsilon_{s(d)}$ given in Table I. The parameters $\tilde{\Lambda}^u_{17}, \tilde{\Lambda}^c_{17}, \tilde{\Lambda}_{78}$ are hadronic parameters that determine the magnitude of the long-distance contribution. Their allowed ranges were updated in Ref. [25] to be as follows:

$$\begin{aligned}-660\ \mathrm{MeV} &< \tilde{\Lambda}^u_{17} < +660\ \mathrm{MeV},\\ -7\ \mathrm{MeV} &< \tilde{\Lambda}^c_{17} < +10\ \mathrm{MeV},\\ 17\ \mathrm{MeV} &< \tilde{\Lambda}_{78} < 190\ \mathrm{MeV}.\end{aligned} \tag{4}$$

The short-distance contributions to $\mathcal{A}_{X_{s(d)}\gamma}$ are the terms that are independent of Λ_{ij}, and $\mathcal{A}^0_{X_{s(d)}\gamma} = \mathcal{A}^{\pm}_{X_{s(d)}\gamma}$ if long-distance terms are neglected. Other parameters are as follows: $\Lambda_c = 0.38$ GeV, $\epsilon_s = (V_{ub}V^*_{us})/(V_{tb}V^*_{ts}) = \lambda^2(i\bar{\eta}-\bar{\rho})/[1-\lambda^2(1-\bar{\rho}+i\bar{\eta})]$ (in terms of Wolfenstein parameters), and $\epsilon_d = (V_{ub}V^*_{ud})/(V_{tb}V^*_{td}) = (\bar{\rho}-i\bar{\eta})/(1-\bar{\rho}+i\bar{\eta})$. The C_i's are Wilson coefficients of relevant operators that are listed in Ref. [10]. In the SM the Wilson coefficients are real and the only term in $\mathcal{A}_{X_{s(d)}\gamma}$ that is nonzero is the term with $\epsilon_{s(d)}$. Due to ϵ_s being of order λ^2 while ϵ_d is of order 1, for the imaginary parts one has $\mathrm{Im}(\epsilon_d)/\mathrm{Im}(\epsilon_s) \approx -22$. For the short-distance contribution only [i.e., neglecting the term with $(\Lambda^u_{17}-\Lambda^c_{17})/m_b$ in Eq. (3)] one has $\mathcal{A}_{X_s\gamma} \approx 0.5\%$ and $\mathcal{A}_{X_d\gamma} \approx 10\%$. The small value of $\mathcal{A}_{X_s\gamma}$ in the SM suggests that this observable could probe models of physics beyond the SM that contain Wilson coefficients with an imaginary part.

TABLE I. The choices of e_{spec} and $\epsilon_{s(d)}$ in the generic formula for $\mathcal{A}_{X_{s(d)}\gamma}$ that give rise to the four asymmetries.

$\mathcal{A}_{X_{s(d)}\gamma}$	e_{spec}	$\epsilon_{s(d)}$
$\mathcal{A}^0_{X_s\gamma}$	$-\frac{1}{3}$	ϵ_s
$\mathcal{A}^{\pm}_{X_s\gamma}$	$\frac{2}{3}$	ϵ_s
$\mathcal{A}^0_{X_d\gamma}$	$-\frac{1}{3}$	ϵ_d
$\mathcal{A}^{\pm}_{X_d\gamma}$	$\frac{2}{3}$	ϵ_d

After the publication of Ref. [10], several works calculated $\mathcal{A}_{X_s\gamma}$ (for the short-distance contribution only) in the context of specific models of physics beyond the SM [26], usually in supersymmetric extensions of it. Values of $\mathcal{A}_{X_s\gamma}$ of up to $\pm 16\%$ were shown to be possible in specific models, while complying with stringent constraints from electric dipole moments (EDMs). Including the long-distance contributions, it was shown in Ref. [24] that the SM prediction using Eq. (3) is enlarged to the range $-0.6\% < \mathcal{A}_{X_s\gamma} < 2.8\%$, and (using updated estimates of the Λ_{ij} parameters) is further increased to $-1.9\% < \mathcal{A}_{X_s\gamma} < 3.3\%$ in Ref. [25]. This revised SM prediction has decreased the effectiveness of $\mathcal{A}_{X_s\gamma}$ as a probe of physics beyond the SM. Consequently, in Ref. [24] the difference of CP asymmetries for the charged and neutral B mesons $\Delta\mathcal{A}_{X_s\gamma} = \mathcal{A}^{\pm}_{X_s\gamma} - \mathcal{A}^0_{X_s\gamma}$ was proposed, which is given by

$$\Delta\mathcal{A}_{X_s\gamma} \approx 4\pi^2\alpha_s\frac{\tilde{\Lambda}_{78}}{m_b}\mathrm{Im}\frac{C_{8g}}{C_{7\gamma}}. \tag{5}$$

This formula is obtained from Eq. (3) in which only the terms with e_{spec} do not cancel out. The SM prediction is $\Delta\mathcal{A}_{X_s\gamma} = 0$ (due to the Wilson coefficients being real) and hence this observable is potentially a more effective probe of new physics than $\mathcal{A}_{X_s\gamma}$. Note that $\Delta\mathcal{A}_{X_s\gamma}$ depends on the product of a long-distance term ($\tilde{\Lambda}_{78}$, whose value is only known to within an order of magnitude) and two short-distance terms (C_8 and C_7).

An alternative observable is the untagged (fully inclusive) asymmetry given by

$$A_{X_{s+d}\gamma} = \frac{(A^0_{X_s\gamma}+r_{0\pm}A^{\pm}_{X_s\gamma})+R_{ds}(A^0_{X_d\gamma}+r_{0\pm}A^{\pm}_{X_d\gamma})}{(1+r_{0\pm})(1+R_{ds})}. \tag{6}$$

Here R_{ds} is the ratio $\mathrm{BR}(\bar{B}\to d\gamma)/\mathrm{BR}(\bar{B}\to s\gamma) \approx |V_{td}/V_{ts}|^2$. The parameter $r_{0\pm}$ is defined as the following ratio:

$$r_{0\pm} \equiv \frac{N^+_{X_s}+N^-_{X_s}}{N^0_{X_s}+N^0_{X_s}}, \tag{7}$$

TABLE II. Measurements (given as a percentage) of $\mathcal{A}_{X_s\gamma}^{\rm tot}$, $\mathcal{A}_{CP}(\bar{B}\to X_{s+d}\gamma)$, and $\Delta\mathcal{A}_{X_s\gamma}$ at BELLE, *BABAR*, and the world average.

	BELLE	*BABAR*	World average
$\mathcal{A}_{X_s\gamma}^{\rm tot}$	$(1.44\pm1.28\pm0.11)\%$ [30]	$(1.73\pm1.93\pm1.02)\%$ [33]	$1.5\%\pm1.1\%$ [31]
$\mathcal{A}_{CP}(\bar{B}\to X_{s+d}\gamma)$	$(2.2\pm3.9\pm0.9)\%$ [34]	$(5.7\pm6.0\pm1.8)\%$ [12]	$1.0\%\pm3.1\%$ [31]
$\Delta\mathcal{A}_{X_s\gamma}$	$(3.69\pm2.65\pm0.76)\%$ [30]	$(5.0\pm3.9\pm1.5)\%$ [33]	$4.1\%\pm2.3\%$ [31]

where $N_{X_s}^+$ is the number of B^+ mesons that decay to $X_s\gamma$, etc. Experimentally, $r_{0\pm}\approx 1.03$ [19] and in our numerical analysis we take $r_{0\pm}=1$. In the fully inclusive measurement of $\mathrm{BR}(b\to s/d\gamma)$ the asymmetry $\mathcal{A}_{CP}(\bar{B}\to X_{s+d}\gamma)$ is measured by counting the difference in the number of positively and negatively charged leptons from the tagged (not signal) B meson. The SM prediction of $\mathcal{A}_{CP}(\bar{B}\to X_{s+d}\gamma)$ is essentially 0 [10,27] (up to tiny m_s^2/m_b^2 corrections), even with the long-distance contribution included. Hence this observable is a cleaner test of new physics than $\mathcal{A}_{X_s\gamma}$. The first studies of the magnitude of the untagged asymmetry in the context of physics beyond the SM were in Ref. [28], and the importance of this observable was emphasized in Ref. [29]. In this work we will consider the above three direct CP asymmetries in the context of 3HDMs: i) $\mathcal{A}_{X_s\gamma}$, ii) $\mathcal{A}_{CP}(\bar{B}\to X_{s+d}\gamma)$, iii) $\Delta\mathcal{A}_{X_s\gamma}$.

Measurements of all three asymmetries have been carried out, and the most recent BELLE and *BABAR* measurements are summarized in Table II. In Table II the CP asymmetry $\mathcal{A}_{X_s\gamma}^{\rm tot}$ would have the same magnitude as the average $\bar{\mathcal{A}}=(\mathcal{A}_{X_s\gamma}^0+\mathcal{A}_{X_s\gamma}^\pm)/2$ if the production cross-sections of B^+B^- and $B^0\overline{B^0}$ were the same. The BELLE measurement [30] of $\bar{\mathcal{A}}=(0.91\pm1.21\pm0.13)\%$ differs only slightly from the BELLE measurement of $\mathcal{A}_{X_s\gamma}^{\rm tot}$ in Table II. The world averages are taken from Ref. [31]. The given averages for $\mathcal{A}_{X_s\gamma}^{\rm tot}$ and $\Delta\mathcal{A}_{X_s\gamma}$ are obtained from the two displayed measurements in Table II, while the average for $\mathcal{A}_{CP}(\bar{B}\to X_{s+d}\gamma)$ also includes two earlier *BABAR* measurements and the CLEO measurement $(-7.9\pm10.8\pm2.2\%)$ [32].

At BELLE II all three asymmetries will be measured with greater precision [19]. At present around 74 fb^{-1} of integrated luminosity have been accumulated, which is about one-tenth of the integrated luminosity at the BELLE experiment, and about one-sixth that at the *BABAR* experiment. By the end of the year 2021, about 1 ab^{-1} is expected, and thus measurements of $b\to s\gamma$ at BELLE II will then match (or better) in precision those at BELLE and *BABAR*. For an integrated luminosity of 50 ab^{-1} (which is expected to be obtained by the end of the BELLE II experiment around the year 2030), the estimated precision for $\mathcal{A}_{X_s\gamma}^{\rm tot}$ is 0.19%, for $\mathcal{A}_{CP}(\bar{B}\to X_{s+d}\gamma)$ is 0.48% (leptonic tag) and 0.7% (hadronic tag), and for $\Delta\mathcal{A}_{X_s\gamma}$ is 0.3% (sum-of-exclusives) and 1.3% (fully inclusive with hadronic tag, and so it measures a sum of $b\to s\gamma$ and $b\to d\gamma$). These numbers are summarized in Table III, together with the SM predictions. Due to the SM prediction of $\mathcal{A}_{CP}(\bar{B}\to X_{s+d}\gamma)$ being essentially zero, a central value of 2.5% with 0.5% error would constitute a 5σ signal of physics beyond the SM. For $\Delta\mathcal{A}_{X_s\gamma}^{\rm tot}$, whose prediction in the SM is also essentially zero, a central value of 1.5% with 0.3% error would constitute a 5σ signal. Note that the current 2σ allowed range of $\mathcal{A}_{X_s\gamma}^{\rm tot}$ is $-0.7\%<\mathcal{A}_{X_s\gamma}^{\rm tot}<3.7\%$ ($-1.8\%<\mathcal{A}_{X_s\gamma}^{\rm tot}<4.8\%$ at 3σ). Comparing this range with the SM prediction of $-1.9\%<\mathcal{A}_{X_s\gamma}^{\rm tot}<3.3\%$ shows that it is less likely that the observable $\mathcal{A}_{X_s\gamma}^{\rm tot}$ alone could provide a clear signal of physics beyond the SM, e.g., a future central value of above 4.3% (which is outside the current 2σ range) with the expected error of 0.19% would be required to give a 5σ discrepancy from the upper SM prediction of 3.3%.

III. THE DECAYS $\bar{B}\to X_s\gamma$ AND $\bar{B}\to X_{s+d}\gamma$ IN THE 3HDM

In this section the theoretical structure of the 3HDM is briefly introduced, followed by a discussion of the Wilson coefficients. Finally, the expressions for the BRs of $\bar{B}\to X_s\gamma$ and $\bar{B}\to X_d\gamma$ are given.

A. Fermionic couplings of the charged scalars in a 3HDM

In a 3HDM, two $SU(2)\otimes U(1)$ isospin scalar doublets (with hypercharge $Y=1$) are added to the Lagrangian of

TABLE III. SM predictions of $\mathcal{A}_{X_s\gamma}^{\rm tot}$, $\mathcal{A}_{CP}(\bar{B}\to X_{s+d}\gamma)$, and $\Delta\mathcal{A}_{X_s\gamma}$, and expected experimental errors in their measurements at BELLE II with 50 ab^{-1}.

	SM Prediction	Leptonic tag	Hadronic tag	Sum of exclusives
$\mathcal{A}_{X_s\gamma}^{\rm tot}$	$-1.9\%<\mathcal{A}_{X_s\gamma}<3.3\%$	x	x	0.19%
$\mathcal{A}_{CP}(\bar{B}\to X_{s+d}\gamma)$	0	0.48%	0.70%	x
$\Delta\mathcal{A}_{X_s\gamma}$	0	x	1.3%	0.3%

the SM. There are two (physical) charged scalars, and for a more detailed description of the model we refer the reader to Refs. [35,36]. In this work we only consider 3HDMs in which all scalar doublets have VEVs (sometimes called "active doublets"). These models do not provide a dark matter candidate, unlike 3HDMs in which one or two doublets do not obtain a VEV ("inert doublets"), and thus the lightest inert scalar provides a dark matter candidate [37–41]. However, theoretical/experimental motivation for the three active scalar doublets includes:

(i) Insights into a possible solution of the flavor problem (i.e., the mixings and masses of the SM fermions) [42];
(ii) A strongly first-order electroweak phase transition, which occurs in a sizeable parameter space, e.g., see [43] in the context of a 3HDM with two inert doublets, which has essentially the same scalar potential as 3HDMs with three active doublets;
(iii) A greatly increased amount of *CP* violation relative to the SM [42] and a mechanism for generating a baryon asymmetry in the universe via the decay of neutral Higgs bosons [44];
(iv) In the aforementioned 3HDMs with inert doublets, *CP* violation in the inert sector only influences the observable sector through loop effects [45–48], and hence its impact is suppressed with respect to the effects studied in this work (in which the *CP* violating phases enter at tree-level);
(v) The 3HDM with three active doublets is a good benchmark model for investigating the phenomenological effects of a *CP* violating phase in charged Higgs interactions. In 2HDMs there is no *CP* violating phase in the charged Higgs sector.

In order to eliminate tree-level flavor changing neutral currents (FCNCs) that are mediated by scalars, the couplings of the scalar doublets to fermions ("Yukawa couplings") are assumed to be invariant under certain discrete symmetries [a requirement called "natural flavor conservation" (NFC), e.g., see Refs. [3,49]]. Each field in the Yukawa couplings (fermionic singlet fields, fermionic doublet fields, and scalar doublet fields) is assigned a charge under three Z_2 symmetries. Requiring that the Lagrangian is invariant under these three Z_2 symmetries (which are only softly broken by dimension 2 terms in the scalar potential) limits the possible Yukawa couplings such that each fermion receives its mass from, at most, one VEV. In this scenario, the fermionic couplings of the neutral scalars are diagonal when written in terms of the neutral scalar mass eigenstates, and thus FCNCs that are mediated by scalars are absent at tree-level. There are five distinct 3HDMs that have NFC (each having different assignments of charges under the Z_2 symmetries), and these 3HDMs are listed in Table IV. The Lagrangian that describes the interactions of $H_1^\pm$ and $H_2^\pm$ (the two charged scalars of the 3HDM, which we do not order in mass) with the fermions is given as follows:

$$\mathcal{L}_{H^\pm} = -\left\{\frac{\sqrt{2}V_{ud}}{v}\bar{u}(m_d X_1 P_R + m_u Y_1 P_L)dH_1^+ + \frac{\sqrt{2}m_\ell}{v}Z_1\overline{\nu_L}\ell_R H_1^+ + \text{H.c.}\right\}$$
$$+\left\{\frac{\sqrt{2}V_{ud}}{v}\bar{u}(m_d X_2 P_R + m_u Y_2 P_L)dH_2^+ + \frac{\sqrt{2}m_\ell}{v}Z_2\overline{\nu_L}\ell_R H_2^+ + \text{H.c.}\right\}. \tag{8}$$

Here $u(d)$ refers to the up(down)-type quarks, and ℓ refers to the electron, muon, and tau. In a 2HDM there is only one charged scalar, and the parameters X, Y, and Z (with no subscript) are equal to $\tan\beta$ or $\cot\beta$ (where $\tan\beta = v_2/v_1$, the ratio of vacuum expectation values). In contrast, in a 3HDM the X_i, Y_i, and Z_i $(i = 1, 2)$ each depend on four parameters of a unitary matrix U, and thus the phenomenology of $H_1^\pm$ and $H_2^\pm$ can differ from that of $H^\pm$ in a 2HDM. This matrix U connects the charged scalar fields in the weak eigenbasis $(\phi_1^\pm, \phi_2^\pm, \phi_3^\pm)$ with the physical scalar fields $(H_1^\pm, H_2^\pm)$ and the charged Goldstone boson $G^\pm$ as follows:

$$\begin{pmatrix} G^+ \\ H_1^+ \\ H_2^+ \end{pmatrix} = U \begin{pmatrix} \phi_1^+ \\ \phi_2^+ \\ \phi_3^+ \end{pmatrix}. \tag{9}$$

The couplings X_i, Y_i, and Z_i in terms of the elements of U are [36]

$$X_1 = \frac{U_{d2}^\dagger}{U_{d1}^\dagger}, \qquad Y_1 = -\frac{U_{u2}^\dagger}{U_{u1}^\dagger}, \qquad Z_1 = \frac{U_{\ell 2}^\dagger}{U_{\ell 1}^\dagger}, \tag{10}$$

and

TABLE IV. The five versions of the 3HDM with NFC, and the corresponding values of u, d, and ℓ. The choice of $u = 2$ means that the up-type quarks receive their mass from the VEV v_2, and likewise for d (down-type quarks) and ℓ (charged leptons).

	u	d	ℓ
3HDM (type I)	2	2	2
3HDM (type II)	2	1	1
3HDM (lepton-specific)	2	2	1
3HDM (flipped)	2	1	2
3HDM (democratic)	2	1	3

$$X_2 = \frac{U^\dagger_{d3}}{U^\dagger_{d1}}, \qquad Y_2 = -\frac{U^\dagger_{u3}}{U^\dagger_{u1}}, \qquad Z_2 = \frac{U^\dagger_{\ell 3}}{U^\dagger_{\ell 1}}. \tag{11}$$

The values of d, u, and ℓ in these matrix elements are given in Table IV and depend on which of the five distinct 3HDMs (with NFC) is being considered. The choice of $d = 1$, $u = 2$, and $\ell = 3$ indicates that the down-type quarks receive their mass from v_1, the up-type quarks from v_2, and the charged leptons from v_3 (and is called the "democratic 3HDM"). The other possible choices of d, u, and ℓ in a 3HDM are given the same names as the four types of 2HDM.

The elements of the matrix U can be parametrized by four parameters–$\tan\beta$, $\tan\gamma$, θ, and δ–where

$$\tan\beta = v_2/v_1, \qquad \tan\gamma = \sqrt{v_1^2 + v_2^2}/v_3. \tag{12}$$

The angle θ and phase δ can be written explicitly as functions of several parameters in the scalar potential [36]. The explicit form of U is

$$\begin{aligned} U = &\begin{pmatrix} 1 & 0 & 0 \\ 0 & e^{-i\delta} & 0 \\ 0 & 0 & 1 \end{pmatrix} \begin{pmatrix} 1 & 0 & 0 \\ 0 & c_\theta & s_\theta e^{i\delta} \\ 0 & -s_\theta e^{-i\delta} & c_\theta \end{pmatrix} \\ &\times \begin{pmatrix} s_\gamma & 0 & c_\gamma \\ 0 & 1 & 0 \\ -c_\gamma & 0 & s_\gamma \end{pmatrix} \begin{pmatrix} c_\beta & s_\beta & 0 \\ -s_\beta & c_\beta & 0 \\ 0 & 0 & 1 \end{pmatrix} \\ = &\begin{pmatrix} s_\gamma c_\beta & s_\gamma s_\beta & c_\gamma \\ -c_\theta s_\beta e^{-i\delta} - s_\theta c_\gamma c_\beta & c_\theta c_\beta e^{-i\delta} - s_\theta c_\gamma s_\beta & s_\theta s_\gamma \\ s_\theta s_\beta e^{-i\delta} - c_\theta c_\gamma c_\beta & -s_\theta c_\beta e^{-i\delta} - c_\theta c_\gamma s_\beta & c_\theta s_\gamma \end{pmatrix}. \end{aligned} \tag{13}$$

Here s and c denote the sine or cosine of the respective angle. Hence the functional forms of X_i, Y_i, and Z_i in a 3HDM depend on four parameters. As mentioned earlier, this is in contrast to the analogous couplings in the 2HDM for which $\tan\beta$ is the only free coupling parameter.

The parameters X_i, Y_i, and Z_i are constrained (for a specific value of $m_{H_i^\pm}$) by direct searches for $H_i^\pm$ (e.g., at the LHC) and by their effect on low-energy observables in flavor physics. A summary of these constraints can be found in Ref. [36], in which the lightest charged scalar is assumed to give the dominant contribution to the observable being considered. A full study in the context of the 3HDM with both charged scalars contributing significantly has not been performed, and is beyond the scope of this work. The coupling Y_i is most strongly constrained from the process $Z \to b\bar{b}$ from LEP data. For $m_{H^\pm}$ around 100 GeV the constraint is roughly $|Y_i| < 0.8$ (assuming $|X_i| \leq 50$, so that the dominant contribution is from the Y_i coupling), and weakens with increasing mass of the charged scalar. Constraints on the X_i and Z_i are weaker and we take $|X_i| < 50$ and $|Z_i| < 50$ as being representative of these constraints for $m_{H_i^\pm}$ around 100 GeV.

The couplings Z_i do not enter the partial width of $b \to s\gamma$, and only the couplings to quarks are relevant (X_i and Y_i). Consequently, the partial width for $b \to s\gamma$ in type I and the lepton-specific structures (which have identical functional forms for X_i and Y_i due to $u = d$ in Table IV) has the same dependence on the parameters of U. Likewise, the partial width for $b \to s\gamma$ in type II, flipped and democratic structures ($u \neq d$ in Table IV) are the same. The contribution of $H_1^\pm$ and $H_2^\pm$ to $\mathrm{BR}(\bar{B} \to X_s\gamma)$ has been studied in the 3HDM at the leading order (LO) in Ref. [50] (no α_s corrections arising from diagrams with charged scalars) and at next-to-leading order (NLO) in Ref. [51] (α_s corrections arising from diagrams with charged scalars). In Ref. [51] the effect of a nonzero phase δ was not studied, and direct CP asymmetries were not considered. Previous studies of $\mathcal{A}_{X_s\gamma}$ (and $\mathcal{A}_{X_d\gamma}$), but not $\mathcal{A}_{CP}(\bar{B} \to X_{s+d}\gamma)$ and $\Delta\mathcal{A}_{X_s\gamma}$, in models with one charged scalar (e.g., 2HDM, or the lightest $H^\pm$ of a 3HDM or multi-Higgs doublet model) have been carried out in Refs. [21–23,52–54].

B. Wilson coefficients in 3HDM

The direct CP asymmetry given by Eq. (3) is written in terms of Wilson coefficients, which (for B observables) are generally evaluated at the scale of $\mu_b = m_b$. We use the explicit formulae in Ref. [23] for the Wilson coefficients at LO and NLO in the 2HDM, and apply them to the 3HDM (generalizing the expressions to account for the two charged scalars). The effective Hamiltonian relevant for radiative B–decays (with $|\Delta B| = |\Delta S| = 1$) is

$$\mathcal{H}_{\rm eff} = -\frac{4G_F}{\sqrt{2}} V^\star_{ts} V_{tb} \sum_{i=1}^{8} C_i(\mu)\mathcal{O}_i(\mu). \tag{14}$$

The operators $\mathcal{O}_2(\mu)$, $\mathcal{O}_7(\mu)$, and $\mathcal{O}_8(\mu)$ are most important for our purposes, but all eight operators are listed below:

$$\begin{aligned} &\mathcal{O}_1 = (\bar{s}_L\gamma_\mu T^a c_L)(\bar{c}_L\gamma^\mu T_a b_L), \quad \mathcal{O}_2 = (\bar{s}_L\gamma_\mu c_L)(\bar{c}_L\gamma^\mu b_L), \\ &\mathcal{O}_3 = (\bar{s}_L\gamma_\mu b_L)\sum_q (\bar{q}\gamma^\mu q), \quad \mathcal{O}_4 = (\bar{s}_L\gamma_\mu T^a b_L)\sum_q (\bar{q}\gamma^\mu T_a q), \\ &\mathcal{O}_5 = (\bar{s}_L\gamma_\mu\gamma_\nu\gamma_\rho b_L)\sum_q (\bar{q}\gamma^\mu\gamma^\nu\gamma^\rho q), \\ &\mathcal{O}_6 = (\bar{s}_L\gamma_\mu\gamma_\nu\gamma_\rho T^a b_L)\sum_q (\bar{q}\gamma^\mu\gamma^\nu\gamma^\rho T_a q), \\ &\mathcal{O}_7 = \frac{e}{16\pi^2}\bar{m}_b(\mu)(\bar{s}_L\sigma^{\mu\nu} b_R)F_{\mu\nu}, \\ &\mathcal{O}_8 = \frac{g_s}{16\pi^2}\bar{m}_b(\mu)(\bar{s}_L\sigma^{\mu\nu} T^a b_R)G^a_{\mu\nu}, \end{aligned} \tag{15}$$

where T^a ($a = 1, 8$) are $SU(3)$ color generators and g_s and e are the strong and electromagnetic coupling constants.

The LO Wilson coefficients [50] at the matching scale $\mu_W = m_W$ are as follows:

$$C_2^{0,\mathrm{eff}}(\mu_W) = 1, \tag{16}$$

$$C_i^{0,\mathrm{eff}}(\mu_W) = 0 \quad (i = 1, 3, 4, 5, 6), \tag{17}$$

$$C_{7\gamma}^{0,\mathrm{eff}}(\mu_W) = C_{7,SM}^0 + |Y_1|^2 C_{7,Y_1Y_1}^0 + |Y_2|^2 C_{7,Y_2Y_2}^0 + (X_1Y_1^*)C_{7,X_1Y_1}^0 + (X_2Y_2^*)C_{7,X_2Y_2}^0, \tag{18}$$

$$C_{8g}^{0,\mathrm{eff}}(\mu_W) = C_{8,SM}^0 + |Y_1|^2 C_{8,Y_1Y_1}^0 + |Y_2|^2 C_{8,Y_2Y_2}^0 + (X_1Y_1^*)C_{8,X_1Y_1}^0 + (X_2Y_2^*)C_{8,X_2Y_2}^0. \tag{19}$$

Terms with $X_1^*Y_1$, $X_2^*Y_2$, $|X_1|^2$, and $|X_2|^2$ are absent because $m_s = 0$ (as is usually taken) in the effective Hamiltonian. Explicit forms for all C_7^0 and C_8^0 are given in Ref. [23]; those for the SM contribution are functions of m_t^2/m_W^2 while those for $H_1^\pm$ and $H_2^\pm$ are functions of $m_t^2/m_{H_1^\pm}^2$ and $m_t^2/m_{H_2^\pm}^2$, respectively.

The NLO Wilson coefficients at the matching scale are as follows:

$$C_1^{1,\mathrm{eff}}(\mu_W) = 15 + 6\ln\frac{\mu_W^2}{M_W^2}, \tag{20}$$

$$C_4^{1,\mathrm{eff}}(\mu_W) = E_0 + \frac{2}{3}\ln\frac{\mu_W^2}{M_W^2} + |Y_1|^2 E_{H_2} + |Y_2|^2 E_{H_3}, \tag{21}$$

$$C_i^{1,\mathrm{eff}}(\mu_W) = 0 \quad (i = 2, 3, 5, 6), \tag{22}$$

$$C_{7\gamma}^{1,\mathrm{eff}}(\mu_W) = C_{7,SM}^{1,\mathrm{eff}}(\mu_W) + |Y_1|^2 C_{7,Y_1Y_1}^{1,\mathrm{eff}}(\mu_W) + |Y_2|^2 C_{7,Y_2Y_2}^{1,\mathrm{eff}}(\mu_W) + (X_1Y_1^*)C_{7,X_1Y_1}^{1,\mathrm{eff}}(\mu_W) + (X_2Y_2^*)C_{7,X_2Y_2}^{1,\mathrm{eff}}(\mu_W), \tag{23}$$

$$C_{8g}^{1,\mathrm{eff}}(\mu_W) = C_{8,SM}^{1,\mathrm{eff}}(\mu_W) + |Y_1|^2 C_{8,Y_1Y_1}^{1,\mathrm{eff}}(\mu_W) + |Y_2|^2 C_{8,Y_2Y_2}^{1,\mathrm{eff}}(\mu_W) + (X_1Y_1^*)C_{8,X_1Y_1}^{1,\mathrm{eff}}(\mu_W) + (X_2Y_2^*)C_{8,X_2Y_2}^{1,\mathrm{eff}}(\mu_W). \tag{24}$$

Explicit forms for all functions are given in Ref. [23]. Renormalization group running is used to evaluate the Wilson coefficients at the scale $\mu = m_b$.

The partial width for $\bar{B} \to X_s\gamma$ has four distinct parts: i) Short-distance contribution from the $b \to s\gamma$ partonic process (to a given order in perturbation theory); ii) Short-distance contribution from the $b \to s\gamma g$ partonic process; iii) Nonperturbative corrections that scale as $1/m_b^2$ and iv) Nonperturbative corrections that scale as $1/m_c^2$, respectively. The partial width of $\bar{B} \to X_s\gamma$ is as follows:

$$\Gamma(\bar{B} \to X_s\gamma) = \frac{G_F^2}{32\pi^4}|V_{ts}^* V_{tb}|^2 \alpha_{em} m_b^5 \left\{ |\bar{D}|^2 + A + \frac{\delta_\gamma^{NP}}{m_b^2}|\mathrm{C}_7^{0,\mathrm{eff}}(\mu_b)|^2 + \frac{\delta_c^{NP}}{m_c^2}\mathrm{Re}\left[[\mathrm{C}_7^{0,\mathrm{eff}}(\mu_b)]^* \times \left(\mathrm{C}_2^{0,\mathrm{eff}}(\mu_b) - \frac{1}{6}\mathrm{C}_1^{0,\mathrm{eff}}(\mu_b) \right) \right] \right\}. \tag{25}$$

The short-distance contribution is contained in $|\bar{D}|^2$, with $\bar{D}$ given by

$$\bar{D} = \mathrm{C}_7^{0,\mathrm{eff}}(\mu_b) + \frac{\alpha_s(\mu_b)}{4\pi}[\mathrm{C}_7^{1,\mathrm{eff}}(\mu_b) + V(\mu_b)]. \tag{26}$$

The Wilson coefficient $C_7^{0,\mathrm{eff}}(\mu_b)$ is a linear combination of $C_7^{0,\mathrm{eff}}(\mu_W)$, $C_8^{0,\mathrm{eff}}(\mu_W)$, and $C_2^{0,\mathrm{eff}}(\mu_W)$, while $C_7^{1,\mathrm{eff}}(\mu_b)$ is a linear combination of these three LO coefficients as well as the NLO coefficients $C_7^{1,\mathrm{eff}}(\mu_W)$, $C_8^{1,\mathrm{eff}}(\mu_W)$, $C_4^{1,\mathrm{eff}}(\mu_W)$, and $C_1^{1,\mathrm{eff}}(\mu_W)$. The parameter $V(\mu_b)$ is a summation over all the LO Wilson coefficients which are evaluated at the scale $\mu_b = m_b$. The contribution from $b \to s\gamma g$ is contained in A, and the remaining two terms are the nonperturbative contributions. In $|\bar{D}|^2$ there are terms of order α_s^2, but to only keep terms to the NLO order for a consistent calculation (to α_s) the following form is used in Ref. [23]:

$$|\bar{D}|^2 = |C_7^{0,\mathrm{eff}}(\mu_b)|^2\{1 + 2\mathrm{Re}(\Delta\bar{D})\}, \tag{27}$$

$$\Delta\bar{D} = \frac{\bar{D} - C_7^{0,\mathrm{eff}}(\mu_b)}{C_7^{0,\mathrm{eff}}(\mu_b)} = \frac{\alpha_s(\mu_b)}{4\pi}\frac{C_7^{1,\mathrm{eff}}(\mu_b) + V(\mu_b)}{C_7^{0,\mathrm{eff}}(\mu_b)}. \tag{28}$$

The m_b^5 dependence is removed by using the measured value of the semileptonic branching ratio $\mathrm{BR}_{SL} \approx 0.1$ and its partial width Γ_{SL} (which also depends on m_b^5), and $\mathrm{BR}(\bar{B} \to X_s\gamma)$ can be written as follows:

$$\mathrm{BR}(\bar{B} \to X_s\gamma) = \frac{\Gamma(\bar{B} \to X_s\gamma)}{\Gamma_{SL}}\mathrm{BR}_{SL}. \tag{29}$$

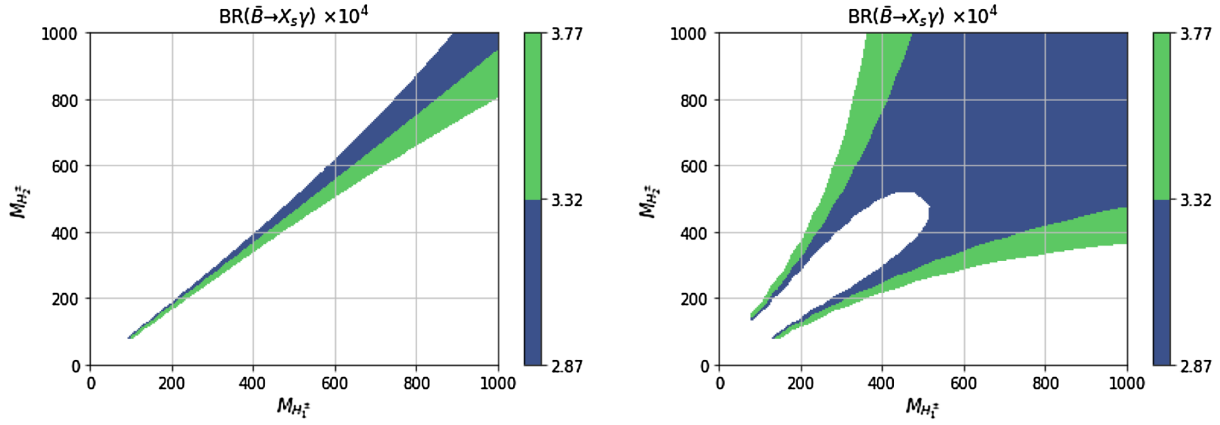

FIG. 1. $\mathrm{BR}(\bar{B} \to X_s\gamma)$ in the plane $[m_{H_1^\pm}, m_{H_2^\pm}]$, with $\theta = -\pi/4$, $\tan\beta = 10$, $\tan\gamma = 1$. Left Panel: $\delta = 0$. Right Panel: $\delta = \pi/2$.

IV. NUMERICAL RESULTS

The four input parameters that determine X_i, Y_i, and Z_i are varied in the following ranges, while respecting the constraints $|X_i| < 50$, $|Z_i| < 50$, and $|Y_i| < 0.8$ for $m_{H_i^\pm} = 100$ GeV:

$$-\pi/2 \le \theta \le 0, \qquad 0 \le \delta \le 2\pi,$$
$$0.1 \le \tan\beta \le 60, \qquad 0.1 \le \tan\gamma \le 60. \tag{30}$$

As mentioned in Sec. III (A), the functional dependence on these four input parameters of the observables $\mathrm{BR}(b \to s\gamma)$, $\mathcal{A}_{X_s\gamma}$, $\mathcal{A}_{CP}(\bar{B} \to X_{s+d}\gamma)$, and $\Delta\mathcal{A}_{X_s\gamma}$ is the same in the flipped 3HDM, type II, and democratic 3HDMs. Results will be shown in this class of models, and sizeable values of the asymmetries are shown to be possible. Results are not shown for the model type I and lepton specific structures because the asymmetries in these two models do not differ much from the SM values, the reason being that the products $X_1 Y_1^*$ and $X_2 Y_2^*$ (which enter the Wilson coefficients) are real in these two models, leading to real C_7 and C_8. The couplings Z_i are different functions of θ, $\tan\beta$, $\tan\gamma$, and δ in the flipped 3HDM, type II, and democratic 3HDMs, and thus the constraints in Eq. (30) on Z_i rule out different regions of the four input parameters in each model. However, the constraints from $Z_i \le 50$ are quite weak, and so the allowed parameter space from $|X_i| < 50$, $|Z_i| < 50$, and $|Y_i| < 0.8$ for $m_{H_i^\pm} = 100$ GeV is essentially the same in all three models under consideration. For definiteness, our results will be presented in the context of the flipped 3HDM. In Eq. (1), for the measurement of $\mathrm{BR}(\bar{B} \to X_s\gamma)$ we take the 3σ allowed range, giving $2.87 \times 10^{-4} \le \mathrm{BR}(\bar{B} \to X_s\gamma) \le 3.77 \times 10^{-4}$.

In Figs. 1(a) and 1(b) the magnitude of $\mathrm{BR}(b \to s\gamma)$ in the plane $[m_{H_1^\pm}, m_{H_2^\pm}]$ is plotted with $\theta = -\pi/4$, $\tan\beta = 10$, and $\tan\gamma = 1$. In the left panel $\delta = 0$ and in the right panel $\delta = \pi/2$. In Ref. [51] only $\delta = 0$ was taken when studying $\mathrm{BR}(b \to s\gamma)$ in 3HDMs. In our numerical analysis we set the normalization scale to be $\mu_b = m_b = 4.77$ GeV (the central value of the b—quark pole mass), and the uncertainty in the asymmetries due to the choice of μ_b is discussed later. It can be seen in Figs. 1(a) and 1(b) that for this choice of parameters the nonzero value of δ significantly increases the allowed parameter space in the plane $[m_{H_1^\pm}, m_{H_2^\pm}]$. In Figs. 2(a) and 2(b) the parameters

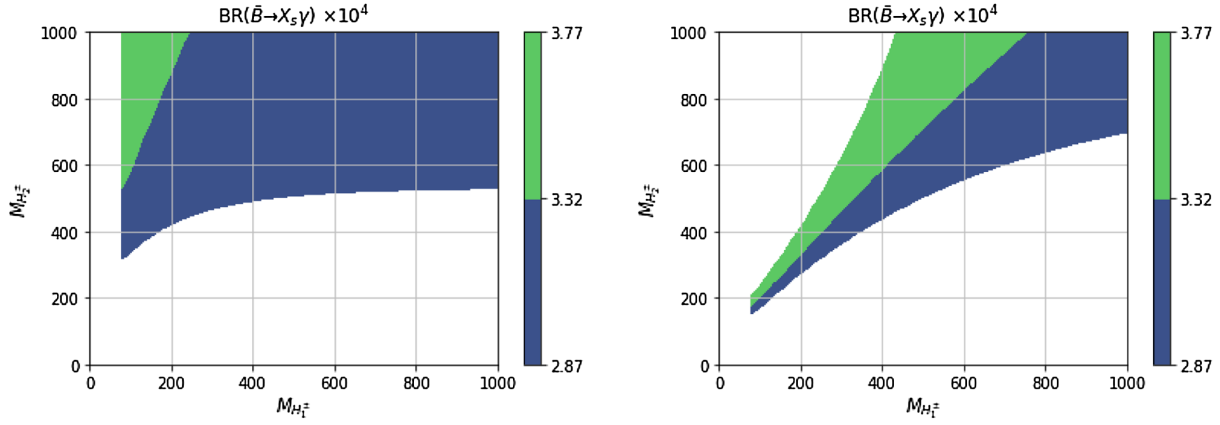

FIG. 2. $\mathrm{BR}(\bar{B} \to X_s\gamma)$ in the plane $[m_{H_1^\pm}, m_{H_2^\pm}]$, with $\theta = -\pi/2.1$, $\tan\beta = 10$, $\tan\gamma = 1$. Left Panel: $\delta = 0$. Right Panel: $\delta = \pi/2$.

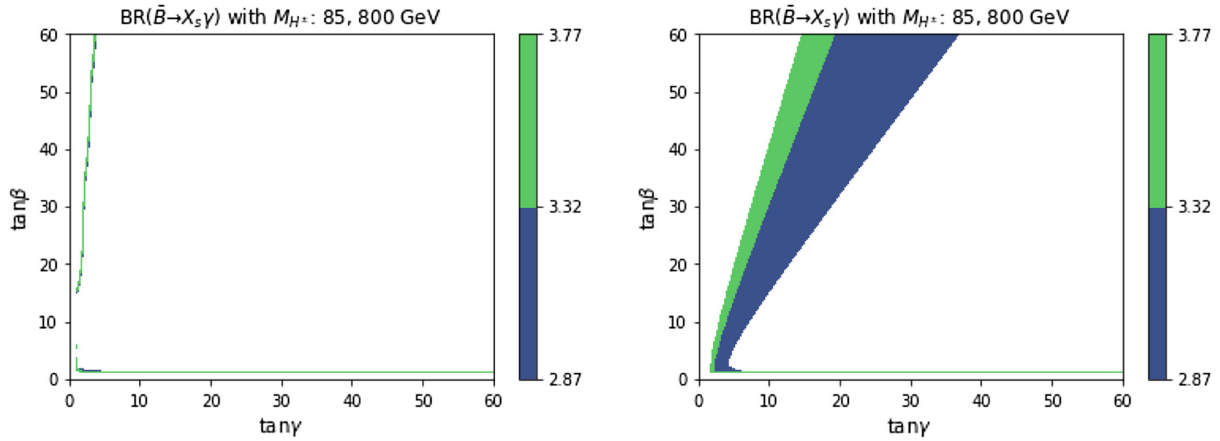

FIG. 3. $\mathrm{BR}(\bar{B}\to X_s\gamma)$ in the plane $[\tan\gamma,\tan\beta]$, with $\theta=-\pi/3$, $m_{H_1^\pm}=85$ GeV, $m_{H_2^\pm}=800$ GeV. Left Panel: $\delta=0$. Right Panel: $\delta=\pi/2$.

are taken to be $\theta=-\pi/2.1$, $\tan\beta=10$, and $\tan\gamma=1$. In the left panel $\delta=0$ and in the right panel $\delta=\pi/2$. In this case the nonzero value of δ significantly decreases the parameter space in the plane $[m_{H_1^\pm},m_{H_2^\pm}]$, although a region with $m_{H_1^\pm}<m_t$ and $m_{H_2^\pm}<m_t$ becomes allowed for $\delta=\pi/2$. In all these plots the notation $m_{H_1^\pm}>m_{H_2^\pm}$ is not used and both masses are scanned in the range $80\ \mathrm{GeV}<m_{H_1^\pm},m_{H_2^\pm}<1000\ \mathrm{GeV}$. It is clear that the phase δ can have a sizeable effect the parameter space of $[m_{H_1^\pm},m_{H_2^\pm}]$ in the 3HDM.

In an earlier work by some of us [55] the region allowed by $\mathrm{BR}(b\to s\gamma)$ in the plane $[\tan\gamma,\tan\beta]$ in the flipped 3HDM was obtained by using the constraint $-0.7<\mathrm{Re}(X_1Y_1^*)<1.1$ only, with $\delta=0$. This is a result from the aligned 2HDM for small $|Y_1|^2$, and when applied to an $H^\pm$ of the 3HDM it is neglecting the contributions of $X_2Y_2^*$, $|Y_2^2|$, and $m_{H_2^\pm}$. In Figs. 3(a) and 3(b) we compare this approximation with the full $\mathrm{BR}(b\to s\gamma)$ constraint in the 3HDM. In Fig. 3(a), the allowed region in the plane $[\tan\gamma,\tan\beta]$ is plotted with $\theta=-\pi/3$, $m_{H_1^\pm}=85$ GeV, and $m_{H_2^\pm}=800$ GeV, with $\delta=0$. The region is much smaller than that displayed in Ref. [55], which used the constraint $-0.7<\mathrm{Re}(X_1Y_1^*)<1.1$ in the same plane; decreasing $m_{H_2^\pm}$ below 600 GeV leads to no allowed parameter space of $[\tan\gamma,\tan\beta]$ for this choice of parameters. In Fig. 3(b), which has $\delta=\pi/2$, but also¿ other parameters the same as those in Fig. 3(a), one can see that the allowed region is much larger, and is in fact more similar in extent (although still smaller) than that allowed from the constraint $-0.7<\mathrm{Re}(X_1Y_1^*)<1.1$ with $\delta=0$ in Ref. [55]. Hence the approximate constraint does not give a very accurate exclusion of parameter space, but the inclusion of a nonzero value of δ can (very roughly) reproduce the allowed regions in Ref. [55] (which focus on the possibility of a large $\mathrm{BR}(H^\pm\to cb)$ in the flipped 3HDM with $\delta=0$). In Figs. 4(a) and 4(b) we take $m_{H_1^\pm}=130$ GeV, $m_{H_2^\pm}=400$ GeV (i.e., a smaller mass splitting between the charged scalars), and $\theta=-\pi/3$.

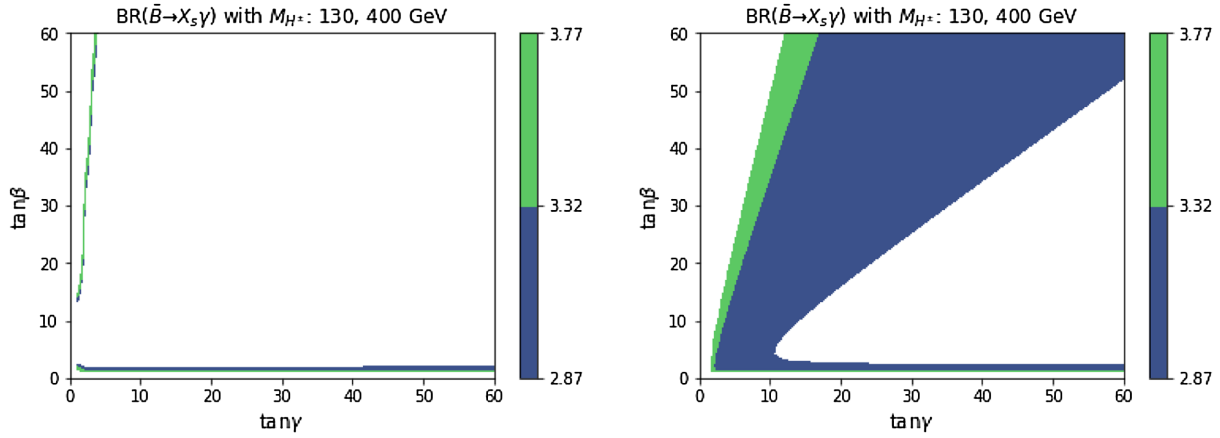

FIG. 4. $\mathrm{BR}(\bar{B}\to X_s\gamma)$ in the plane $[\tan\gamma,\tan\beta]$, with $\theta=-\pi/3$, $m_{H_1^\pm}=130$ GeV, $m_{H_2^\pm}=400$ GeV. Left Panel: $\delta=\pi/4$. Right Panel: $\delta=\pi/2$.

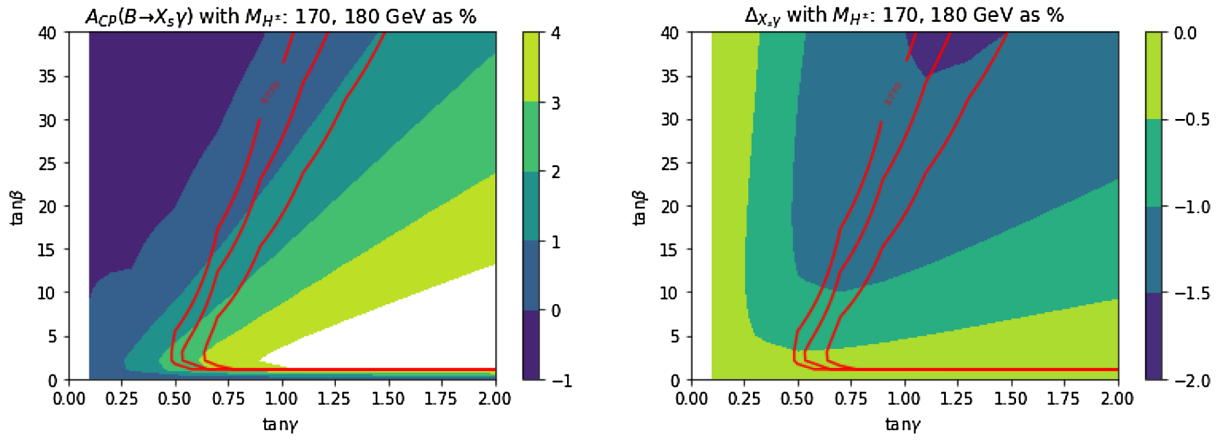

FIG. 5. CP asymmetries (as a percentage) in the plane $[\tan\gamma, \tan\beta]$ with $m_{H_1^\pm} = 170$ GeV, $m_{H_2^\pm} = 180$ GeV, $\theta = -\pi/4$, and $\delta = 2.64$. The three red lines (from left to right) show the upper (3σ) limit, the central value, and the lower (3σ) limit for $\mathrm{BR}(\bar{B} \to X_s\gamma)$. Left Panel: $\mathcal{A}_{CP}(\bar{B} \to X_s\gamma)$, with the white region for $\tan\gamma > 1$ violating the 3σ experimental bounds. Right Panel: ΔA_{CP}.

In Fig. 4(a) we take $\delta = \pi/4$ and in Fig. 4(b) $\delta = \pi/2$. One can see that for $\delta = \pi/4$ very little parameter space is allowed by $\mathrm{BR}(b \to s\gamma)$. In contrast, for $\delta = \pi/2$ a sizeable region of the plane $[\tan\gamma, \tan\beta]$ is permitted. We calculated $\mathrm{BR}(H^\pm \to cb)$ in the same plane $[\tan\gamma, \tan\beta]$ but with $\delta = \pi/2$ and found that is essentially the same as the case with $\delta = 0$ in Ref. [55]. Hence there is a sizeable parameter space for a large $\mathrm{BR}(H^\pm \to cb)$ in the flipped 3HDM while satisfying the full $\mathrm{BR}(b \to s\gamma)$ constraint, provided that δ is nonzero.

We now turn our attention to the CP asymmetries. For $\mathcal{A}_{X_s\gamma}$ we use $\bar{\mathcal{A}} = (\mathcal{A}^0_{X_s\gamma} + \mathcal{A}^\pm_{X_s\gamma})/2$, which is obtained by taking $e_{\mathrm{spec}} = 1/6$. The CP asymmetries are evaluated at $\mathcal{O}(\alpha_s)$ so that we use the LO formulae for the Wilson coefficients C_2, $C_{7\gamma}$, and C_{8g} in Eq. (3). In order to evaluate the CP asymmetries at $\mathcal{O}(\alpha_s^2)$, it is necessary to include not only the NLO terms of these Wilson coefficients but also the NNLO terms of $C_{7\gamma}$ and C_{8g}.

In Figs. 5(a), 5(b), and 6 the asymmetries $\mathcal{A}_{X_s\gamma}$, ΔA_{CP}, and $\mathcal{A}_{CP}(\bar{B} \to X_{s+d}\gamma)$ are (respectively) plotted in the plane $[\tan\gamma, \tan\beta]$. In all these figures the remaining four 3HDM parameters are fixed as $m_{H_1^\pm} = 170$ GeV, $m_{H_2^\pm} = 180$ GeV, $\theta = -\pi/4$, and $\delta = 2.64$, whereas the long-distance (hadronic) parameters are taken to be $\tilde{\Lambda}^u_{17} = 0.66$ GeV, $\tilde{\Lambda}^c_{17} = 0.010$ GeV, and $\tilde{\Lambda}_{78} = 0.19$ GeV.

The scale μ_b is taken to be 4.77 GeV (pole mass m_b). The three red lines (from left to right) show the upper (3σ) limit, the central value, and the lower (3σ) limit for $\mathrm{BR}(\bar{B} \to X_s\gamma)$. The white region in Fig. 5(a) with roughly $\tan\gamma > 1$ violates the current experimental (3σ) limit for $\mathcal{A}_{X_s\gamma}$ (the white regions in Figs. 5(a), 5(b), and 6 with $\tan\gamma < 0.1$ correspond to parameter choices not covered in the scan). In Fig. 5(a), in the parameter space allowed by $\mathrm{BR}(\bar{B} \to X_s\gamma)$, the magnitude of $\mathcal{A}_{X_s\gamma}$ is roughly between 0.5% and 1.5%, which is within the current experimental limits. In Fig. 5(b), ΔA_{CP} can reach -1.5%, which would provide a 5σ signal at BELLE II with 50 ab^{-1}. We note that ΔA_{CP} is directly proportional to $\tilde{\Lambda}_{78}$, which has been taken to have its largest allowed value. If $\tilde{\Lambda}_{78}$ is reduced then ΔA_{CP} will decrease proportionally. In Fig. 6 it is shown that $\mathcal{A}_{CP}(\bar{B} \to X_{s+d}\gamma)$ can reach almost -3%, which would be a 5σ signal at BELLE II. The parameter $\tilde{\Lambda}_{78}$ has a subdominant effect on $\mathcal{A}_{CP}(\bar{B} \to X_{s+d}\gamma)$ (in contrast to ΔA_{CP}) and so $\mathcal{A}_{CP}(\bar{B} \to X_{s+d}\gamma) \approx -3\%$ is possible, independent of the value of $\tilde{\Lambda}_{78}$. We note that there is more parameter space in a 3HDM for such large asymmetries than in the aligned 2HDM [53,54]. This is because there is a greater possibility of cancellation in the contributions of $H_1^\pm$ and $H_2^\pm$ to $\bar{B} \to X_s\gamma$ (while having a large asymmetry), but in

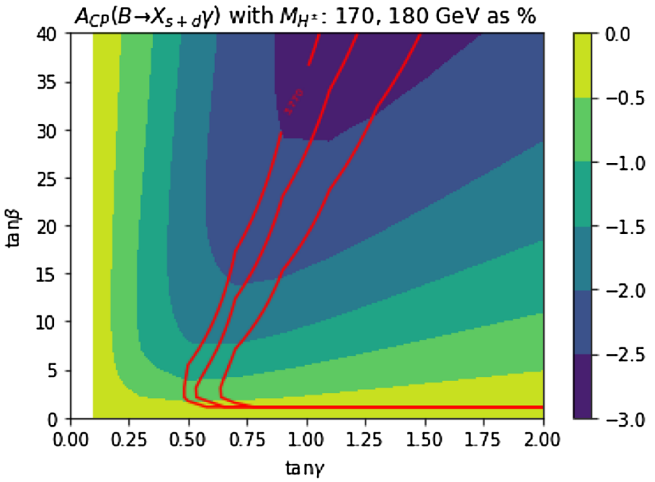

FIG. 6. $\mathcal{A}_{CP}(\bar{B} \to X_{s+d}\gamma)$ (as a percentage) in the plane $[\tan\gamma, \tan\beta]$ with $m_{H_1^\pm} = 170\,\mathrm{GeV}$, $m_{H_2^\pm} = 180\,\mathrm{GeV}$, $\theta = -\pi/4$, and $\delta = 2.64$. The three red lines (from left to right) show the upper (3σ) limit, the central value, and the lower (3σ) limit for $\mathrm{BR}(\bar{B} \to X_s\gamma)$.

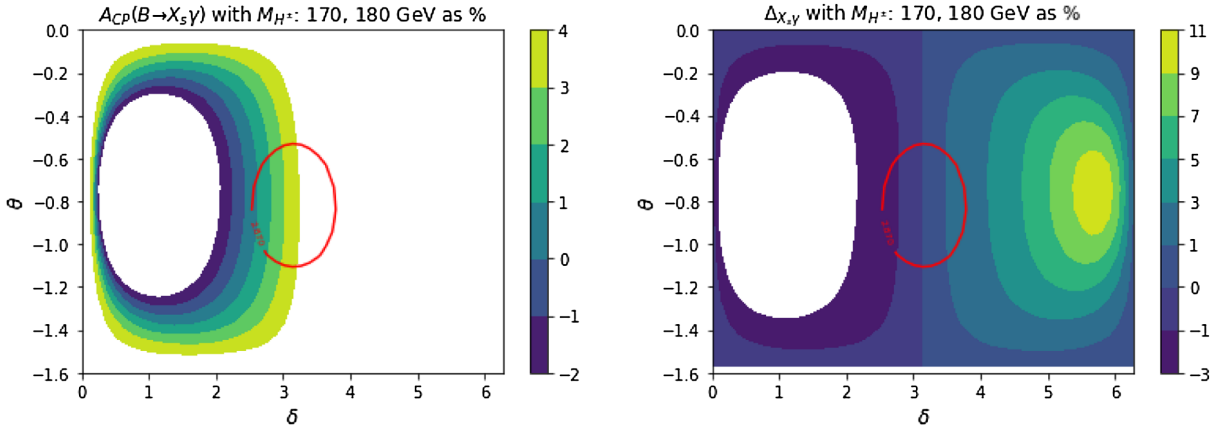

FIG. 7. *CP* asymmetries (as a percentage) in the plane $[\delta, \theta]$ with $m_{H_1^\pm} = 170$ GeV, $m_{H_2^\pm} = 180$ GeV, $\tan\beta = 35$, and $\tan\gamma = 1.32$. Inside the red circles the predicted $\mathrm{BR}(\bar{B} \to X_s\gamma)$ satisfies the current experimental constraint. The white regions are excluded by the current (3σ) experimental limits on the asymmetry displayed in the figure. Left Panel: $\mathcal{A}_{CP}(\bar{B} \to X_s\gamma)$. Right Panel: ΔA_{CP}.

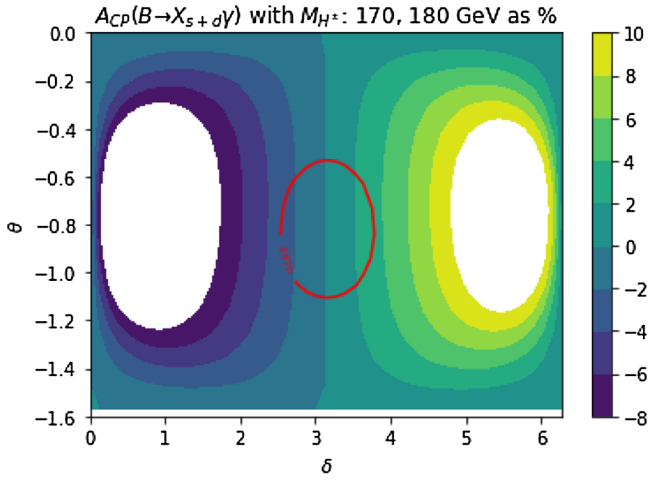

FIG. 8. $\mathcal{A}_{CP}(\bar{B} \to X_{s+d}\gamma)$ (as a percentage) in the plane $[\delta,\ \theta]$ with $m_{H_1^\pm} = 170$ GeV, $m_{H_2^\pm} = 180$ GeV, $\tan\beta = 35$, and $\tan\gamma = 1.32$. Inside the red circle the predicted $\mathrm{BR}(\bar{B} \to X_s\gamma)$ satisfies the current experimental constraint. The white regions are excluded by the current (3σ) experimental limits on $\mathcal{A}_{CP}(\bar{B} \to X_{s+d}\gamma)$.

the aligned 2HDM there is only one charged scalar and no X_2 and Y_2 coupling.

In Figs. 7(a), 7(b), and 8 the contours of the *CP* asymmetries are shown in the plane $[\delta, \theta]$. The other parameters are fixed as $m_{H_1^\pm} = 170\,\mathrm{GeV}$, $m_{H_2^\pm} = 180\,\mathrm{GeV}$, $\tan\beta = 35$, and $\tan\gamma = 1.32$. The scale μ_b and the hadronic parameters are taken to be the same as in Figs. 5(a), 5(b), and 6. Inside the red circles the predicted $\mathrm{BR}(\bar{B} \to X_s\gamma)$ satisfies the current (3σ) experimental constraint, and restricts the allowed parameter space to be roughly $2.5 < \delta < 3.5$ and $-0.5 < \theta < -1.1$ (i.e., an ellipse centred on around $\delta = 3$). The white regions in all plots violate the current 3σ experimental limits (see Table II) on the displayed asymmetry. In Fig. 7(a) it can be seen that roughly the right half $(\delta > 3)$ of the ellipse is ruled out from $\mathcal{A}_{CP}(\bar{B} \to X_s\gamma)$. In Figs. 7(b) and 8, in the allowed region of the plane $[\delta, \theta]$ the asymmetries increase in magnitude as δ is varied from $\delta = \pi$ to $\delta \approx 2.5$, and values of $\Delta A_{CP} \approx -1.5\%$ and $\mathcal{A}_{CP}(\bar{B} \to X_{s+d}\gamma) \approx -3\%$ can again be reached. The theoretical uncertainty is significant, and will be quantified in what follows.

We now consider the theoretical uncertainty of our predictions that arise from varying the scale μ_b and the hadronic parameters. In Tables V, VI, and VII the parameters are fixed as $m_{H_1^\pm} = 170$ GeV, $m_{H_2^\pm} = 180$ GeV, $\theta = -\frac{\pi}{4}$, and $\delta = 2.64$ [the same as in Figs. 5(a), 5(b), and 6]. Also, $\tan\beta = 35$ and $\tan\gamma = 1.32$ (the same as in Figs. 7(a), 7(b), and 8). Table V uses the lowest possible values of the hadronic parameters, Table VI uses the central values, and Table VII uses the maximum values. In each

TABLE V. Dependence of the asymmetries on the scale μ_b, taking the lowest values of the hadronic parameters and $m_b = 4.71$ GeV. Parameters are fixed as follows: $m_{H_1^\pm} = 170$ GeV, $m_{H_2^\pm} = 180$ GeV, $\theta = -\frac{\pi}{4}$, $\tan\beta = 35$, $\tan\gamma = 1.32$, $\delta = 2.64$, $\tilde{\Lambda}_{17}^u = -0.66$ GeV, $\tilde{\Lambda}_{17}^c = -0.007$ GeV, $\tilde{\Lambda}_{78} = 0.017$ GeV with LO C_7, C_8.

μ_b	$\bar{B} \to s\gamma(\times 10^{-4})$	$\mathcal{A}_{CP}(\bar{B} \to X_s\gamma)\%$	$\Delta A_{CP}\%$	$\mathcal{A}_{CP}(\bar{B} \to X_{s+d}\gamma)\%$
$m_b/2$	2.912	−3.170	−0.111	−0.974
m_b	2.968	−3.636	−0.134	−1.058
$2m_b$	2.801	−4.137	−0.163	−1.153

TABLE VI. Dependence of the asymmetries on the scale μ_b, taking the central values of the hadronic parameters and $m_b = 4.77$ GeV. Parameters are fixed as follows: $m_{H_1^\pm} = 170$ GeV, $m_{H_2^\pm} = 180$ GeV, $\theta = -\frac{\pi}{4}$, $\tan\beta = 35$, $\tan\gamma = 1.32$, $\delta = 2.64$, $\tilde{\Lambda}_{17}^u = 0$ GeV, $\tilde{\Lambda}_{17}^c = 0.0085$ GeV, $\tilde{\Lambda}_{78} = 0.0865$ GeV with LO C_7, C_8.

μ_b	$\bar{B} \to s\gamma(\times 10^{-4})$	$\mathcal{A}_{CP}(\bar{B} \to X_s\gamma)\%$	$\Delta A_{CP}\%$	$\mathcal{A}_{CP}(\bar{B} \to X_{s+d}\gamma)\%$
$m_b/2$	2.888	−1.220	−0.562	−1.755
m_b	2.931	−1.663	−0.673	−2.151
$2m_b$	2.761	−2.212	−0.820	−2.670

TABLE VII. Dependence of the asymmetries on the scale μ_b, taking the largest values of the hadronic parameters and $m_b = 4.83$ GeV. Parameters are fixed as follows: $m_{H_1^\pm} = 170$ GeV, $m_{H_2^\pm} = 180$ GeV, $\theta = -\frac{\pi}{4}$, $\tan\beta = 35$, $\tan\gamma = 1.32$, $\delta = 2.64$ $\tilde{\Lambda}_{17}^u = 0.66$ GeV, $\tilde{\Lambda}_{17}^c = 0.010$ GeV, $\tilde{\Lambda}_{78} = 0.19$ GeV with LO C_7, C_8.

μ_b	$\bar{B} \to s\gamma(\times 10^{-4})$	$\mathcal{A}_{CP}(\bar{B} \to X_s\gamma)\%$	$\Delta A_{CP}\%$	$\mathcal{A}_{CP}(\bar{B} \to X_{s+d}\gamma)\%$
$m_b/2$	2.865	1.145	−1.223	−2.123
m_b	2.896	0.914	−1.466	−2.641
$2m_b$	2.724	0.581	−1.7854	−3.323

TABLE VIII. Contributions to $\mathcal{A}_{CP}(\bar{B} \to X_{s+d}\gamma)$ from the terms proportional to $\mathrm{Im}(C_2/C_{7\gamma})$, $\mathrm{Im}(C_{8g}/C_{7\gamma})$, and $\mathrm{Im}(\epsilon_{s(d)}C_2/C_{7\gamma})$ in Eq. (3) for three benchmark points, which correspond to the lowest (BP1), central (BP2), and largest (BP3) values of the hadronic parameters and m_b, with $\mu_b = m_b$. Other parameters are fixed as follows: $m_{H_1^\pm} = 170$ GeV, $m_{H_2^\pm} = 180$ GeV, $\theta = -\frac{\pi}{4}$, $\tan\beta = 35$, $\tan\gamma = 1.32$, $\delta = 2.64$ with LO C_7, C_8.

	$\mathrm{Im}(C_2/C_{7\gamma})$	$\mathrm{Im}(C_{8g}/C_{7\gamma})$	$\mathrm{Im}(\epsilon_{s(d)}C_2/C_{7\gamma})$	$\mathcal{A}_{CP}(\bar{B} \to X_{s+d}\gamma)\%$
BP1 (lowest)	−1.638	0.395	0.185	−1.058
BP2 (central)	−2.422	0.306	−0.035	−2.151
BP3 (largest)	−2.559	0.176	−0.258	−2.641

table the value of the scale μ_b is taken to be $\mu_b = m_b/2$, m_b, and $2m_b$. The pole b—quark mass is 4.77 ± 0.06 GeV, and in Tables V, VI, and VII we take 4.71 GeV, 4.77 GeV, and 4.83 GeV, respectively. This scale dependence corresponds to the NNLO contributions in $\mathrm{BR}(\bar{B} \to X_s\gamma)$ and the NLO contributions in the CP asymmetries. The uncertainty from μ_b is around 50% for ΔA_{CP} and $\mathcal{A}_{CP}(\bar{B} \to X_{s+d}\gamma)$ in each table. One can see that increasing the scale μ_b makes both ΔA_{CP} and $\mathcal{A}_{CP}(\bar{B} \to X_{s+d}\gamma)$ more negative. The CP asymmetry $A_{CP}(\bar{B} \to X_s\gamma)$ is very significantly affected by the change of the hadronic parameters, so that even the sign of the asymmetry is flipped. The effect of the change of the hadronic parameters on ΔA_{CP} is also severe (due to it being proportional to $\tilde{\Lambda}_{78}$), while the effect on $\mathcal{A}_{CP}(\bar{B} \to X_{s+d}\gamma)$ is less significant. The maximum and minimum values of the observables in Tables V, VI, and VII are as follows:

$$2.724 \times 10^{-4} < \mathrm{BR}(\bar{B} \to X_s\gamma) < 2.968 \times 10^{-4}, \quad (31)$$

$$-4.137\% < \mathcal{A}_{CP}(\bar{B} \to X_s\gamma) < 0.581\%, \quad (32)$$

$$-1.785\% < \Delta A_{CP} < -0.111\%, \quad (33)$$

$$-3.323\% < \mathcal{A}_{CP}(\bar{B} \to X_{s+d}\gamma) < -0.974\%. \quad (34)$$

We note that a full scan over the hadronic parameters might result in larger asymmetries.

In Table VII the contributions to the untagged asymmetry $\mathcal{A}_{CP}(\bar{B} \to X_{s+d}\gamma)$ from the terms proportional to $\mathrm{Im}(C_2/C_{7\gamma})$, $\mathrm{Im}(C_{8g}/C_{7\gamma})$, and $\mathrm{Im}(\epsilon_{s(d)}C_2/C_{7\gamma})$ in Eq. (3) are displayed. The benchmark points BP1, BP2, and BP3, respectively, correspond to the lowest, central, and largest values of the hadronic parameters and m_b, with $\mu_b = m_b$. The other parameters are fixed to the same values as in Tables V, VI, and VII. The value of $\mathcal{A}_{CP}(\bar{B} \to X_{s+d}\gamma)$ in BP1, BP2, and BP3 is therefore equal to its value in the middle rows of Tables V, VI, and VII, respectively. For these benchmark points it can be seen that the dominant contribution to the untagged asymmetry comes from $\mathrm{Im}(C_2/C_{7\gamma})$.

A. Electric dipole moments, collider limits, and theoretical consistency

In a separate publication [56] some of us addressed the calculation of both the neutron and electron EDMs in the 3HDM discussed here, as these observables will be affected

by a nonzero value of the CP violating (CPV) phase δ. Without preempting the results to appear therein, it has been checked that the regions of 3HDM parameter space explored in our present analysis are generally compliant with constraints coming from both neutron and electron EDMs. However, some regions of the parameter space covered here would be excluded. Specifically, with reference to the $\tan\beta$ and $\tan\gamma$ values adopted and the $[\delta, \theta]$ plane considered, we can anticipate that the regions centred around $\theta \approx -0.8$ and $\delta \approx 1.4$ and 4.6 would be excluded by the combination of the two EDMs. However, the expanse of such an invalid parameter space diminishes significantly as $m_{H_1^\pm}$ and $m_{H_2^\pm}$ get closer, to the extent that no limits can be extracted from such observables in the case of exact mass degeneracy of the two charged Higgs states for suitable values of their Yukawa couplings. Hence, the majority of the results presented here are stable against EDM constraints. Indeed, it should further be noted that both in the present paper and in Ref. [56], for computational reasons, the neutral Higgs sector of the 3HDM has essentially been decoupled. Hence, in the case of a lighter neutral scalar spectrum one may potentially invoke cancellations occurring between the charged and neutral Higgs boson states (including the SM-like one) of the CPV 3HDM (in the same spirit as those of Ref. [57] for the CPV aligned 2HDM), which could further reduce the impact of EDM constraints. Moreover, one also ought to make sure that the $H_1^\pm$ and $H_2^\pm$ spectra of masses and couplings adopted here do not violate bounds coming from colliders, specifically LEP/SLC, Tevatron and the LHC. Again, based on the forthcoming results of Ref. [56], we anticipate this being the case in the present context. Finally, in Ref. [56], it will also be shown that the values of the Yukawa parameters adopted in this paper are compliant with theoretical self-consistency requirements of the 3HDM stemming from vacuum stability and perturbativity.

V. CONCLUSIONS

In the context of 3HDMs with NFC, the magnitudes of three CP asymmetries that involve the decay $b \to s/d\gamma$ have been studied. In the SM, the CP asymmetry in the inclusive decay $\bar{B} \to X_s\gamma$ alone ($\mathcal{A}_{X_s\gamma}$) has a theoretical error from long-distance contributions that render it unlikely to provide a clear signal of physics beyond the SM at the ongoing BELLE II experiment. The untagged asymmetry ($\mathcal{A}_{CP}(\bar{B} \to X_{s+d}\gamma)$) and the difference of CP asymmetries ($\Delta\mathcal{A}_{X_s\gamma}$) are both predicted to be essentially zero in the SM, with negligible theoretical error. Hence these latter two observables offer better prospects of revealing new physics contributions to $b \to s/d\gamma$.

In the context of 3HDMs there are two charged scalars that contribute to the process $b \to s/d\gamma$. There are six new physics parameters (two masses of the charged scalars and four parameters that determine the Yukawa couplings of the charged scalars) that together enable the relevant Wilson coefficients to contain a sizeable imaginary part. In three of the five types of 3HDM the magnitude of $\mathcal{A}_{CP}(\bar{B} \to X_{s+d}\gamma)$ and $\Delta\mathcal{A}_{X_s\gamma}$ can reach values such that a 5σ signal at the BELLE II experiment with 50 ab^{-1} of integrated luminosity would be possible. Although the parameter space for such a clear signal is rather small (which is also usually the case in other models of physics beyond the SM), it was shown that a 3HDM could accommodate any such signal, and thus would be a candidate model for a statistically significant excess (beyond the SM prediction) in these asymmetry observables.

ACKNOWLEDGMENTS

A. A. and S. M. are supported in part through the STFC Consolidated Grant No. ST/L000296/1. S. M. is supported in part through the NExT Institute. S. M. and M. S. acknowledge the H2020-MSCA-RISE-2014 Grant No. 645722 (NonMinimalHiggs). T. S. is supported in part by JSPS KAKENHI Grant No. 20H00160. T. S. and S. M. are partially supported by the Kogakuin University Grant for the project research "Phenomenological study of new physics models with extended Higgs sector". We thank H. E. Logan and D. Rojas-Ciofalo for reading the manuscript and for useful comments.

[1] G. Aad *et al.* (ATLAS Collaboration), Phys. Lett. B **716**, 1 (2012).
[2] S. Chatrchyan *et al.* (CMS Collaboration), Phys. Lett. B **716**, 30 (2012).
[3] G. C. Branco, P. M. Ferreira, L. Lavoura, M. N. Rebelo, M. Sher, and J. P. Silva, Phys. Rep. **516**, 1 (2012).
[4] A. G. Akeroyd *et al.*, Eur. Phys. J. C **77**, 276 (2017).
[5] S. Weinberg, Phys. Rev. Lett. **37**, 657 (1976); C. H. Albright, J. Smith, and S. H. H. Tye, Phys. Rev. D **21**, 711 (1980); G. C. Branco, A. J. Buras, and J. M. Gerard, Nucl. Phys. **B259**, 306 (1985).
[6] Y. Grossman, Nucl. Phys. **B426**, 355 (1994).
[7] A. G. Akeroyd and W. J. Stirling, Nucl. Phys. **B447**, 3 (1995).
[8] A. G. Akeroyd, S. Moretti, and J. Hernandez-Sanchez, Phys. Rev. D **85**, 115002 (2012).
[9] M. Misiak, H. M. Asatrian, R. Boughezal, M. Czakon, T. Ewerth, A. Ferroglia, P. Fiedler, P. Gambino, C. Greub,

U. Haisch, T. Huber, M. Kaminski, G. Ossola, M. Poradzinski, A. Rehman, T. Schutzmeier, M. Steinhauser, and J. Virto, Phys. Rev. Lett. **114**, 221801 (2015).
[10] A. L. Kagan and M. Neubert, Phys. Rev. D **58**, 094012 (1998).
[11] S. Chen *et al.* (CLEO Collaboration), Phys. Rev. Lett. **87**, 251807 (2001).
[12] J. P. Lees *et al.* (*BABAR* Collaboration), Phys. Rev. D **86**, 112008 (2012); Phys. Rev. Lett. **109**, 191801 (2012).
[13] A. Abdesselam *et al.* (Belle Collaboration), arXiv: 1608.02344.
[14] B. Aubert *et al.* (*BABAR* Collaboration), Phys. Rev. D **77**, 051103 (2008).
[15] J. P. Lees *et al.* (*BABAR* Collaboration), Phys. Rev. D **86**, 052012 (2012).
[16] T. Saito *et al.* (Belle Collaboration), Phys. Rev. D **91**, 052004 (2015).
[17] P. del Amo Sanchez *et al.* (*BABAR* Collaboration), Phys. Rev. D **82**, 051101 (2010).
[18] Y. S. Amhis *et al.* (HFLAV Collaboration), arXiv:1909 .12524.
[19] E. Kou *et al.* (Belle-II Collaboration), Prog. Theor. Exp. Phys. (**2019**), 123C01.
[20] M. Misiak, A. Rehman, and M. Steinhauser, J. High Energy Phys. 06 (2020) 175.
[21] L. Wolfenstein and Y. L. Wu, Phys. Rev. Lett. **73**, 2809 (1994); Y. L. Wu, Chin. Phys. Lett. **16**, 339 (1999).
[22] G. M. Asatrian and A. Ioannisian, Phys. Rev. D **54**, 5642 (1996); H. M. Asatrian, G. K. Egiian, and A. N. Ioannisian, Phys. Lett. B **399**, 303 (1997).
[23] F. Borzumati and C. Greub, Phys. Rev. D **58**, 074004 (1998).
[24] M. Benzke, S. J. Lee, M. Neubert, and G. Paz, Phys. Rev. Lett. **106**, 141801 (2011).
[25] A. Gunawardana and G. Paz, J. High Energy Phys. 11 (2019) 141.
[26] C. K. Chua, X. G. He, and W. S. Hou, Phys. Rev. D **60**, 014003 (1999); Y. G. Kim, P. Ko, and J. S. Lee, Nucl. Phys. **B544**, 64 (1999); M. Aoki, G. C. Cho, and N. Oshimo, Phys. Rev. D **60**, 035004 (1999); L. Giusti, A. Romanino, and A. Strumia, Nucl. Phys. **B550**, 3 (1999); S. Baek and P. Ko, Phys. Rev. Lett. **83**, 488 (1999); T. Goto, Y. Y. Keum, T. Nihei, Y. Okada, and Y. Shimizu, Phys. Lett. B **460**, 333 (1999); M. Aoki, G. C. Cho, and N. Oshimo, Nucl. Phys. **B554**, 50 (1999); T. Goto, Y. Okada, Y. Shimizu, T. Shindou, and M. Tanaka, Phys. Rev. D **70**, 035012 (2004).
[27] J. M. Soares, Nucl. Phys. **B367**, 575 (1991).
[28] A. G. Akeroyd, Y. Y. Keum, and S. Recksiegel, Phys. Lett. B **507**, 252 (2001); A. G. Akeroyd and S. Recksiegel, Phys. Lett. B **525**, 81 (2002).
[29] T. Hurth, E. Lunghi, and W. Porod, Nucl. Phys. **B704**, 56 (2005).
[30] S. Watanuki *et al.* (Belle Collaboration), Phys. Rev. D **99**, 032012 (2019).
[31] M. Tanabashi *et al.* (Particle Data Group), Phys. Rev. D **98**, 030001 (2018).
[32] T. E. Coan *et al.* (CLEO Collaboration), Phys. Rev. Lett. **86**, 5661 (2001).
[33] J. P. Lees *et al.* (*BABAR* Collaboration), Phys. Rev. D **90**, 092001 (2014).
[34] L. Pesntez *et al.* (Belle Collaboration), Phys. Rev. Lett. **114**, 151601 (2015).
[35] A. G. Akeroyd, S. Moretti, and M. Song, Phys. Rev. D **101**, 035021 (2020).
[36] G. Cree and H. E. Logan, Phys. Rev. D **84**, 055021 (2011).
[37] V. Keus, S. F. King, S. Moretti, and D. Sokolowska, J. High Energy Phys. 11 (2014) 016.
[38] V. Keus, S. F. King, S. Moretti, and D. Sokolowska, J. High Energy Phys. 11 (2015) 003.
[39] A. Cordero, J. Hernandez-Sanchez, V. Keus, S. F. King, S. Moretti, D. Rojas, and D. Sokolowska, J. High Energy Phys. 05 (2018) 030.
[40] D. Rojas-Ciofalo, A. Cordero, J. Hernandez-Sanchez, V. Keus, S. Moretti, and D. Sokolowska, Proc. Sci., LHCP2019 (**2019**) 013. [arXiv:1907.12522].
[41] A. Aranda, D. Hernandez-Otero, J. Hernandez-Sanchez, V. Keus, S. Moretti, D. Rojas-Ciofalo, and T. Shindou, arXiv: 1907.12470.
[42] G. C. Branco, D. Das, M. Levy, and P. B. Pal, Phys. Rev. D **102**, 035007 (2020).
[43] A. Ahriche, G. Faisel, S. Y. Ho, S. Nasri, and J. Tandean, Phys. Rev. D **92**, 035020 (2015).
[44] H. Davoudiasl, I. M. Lewis, and M. Sullivan, Phys. Rev. D **101**, 055010 (2020).
[45] V. Keus, S. F. King, S. Moretti, and K. Yagyu, J. High Energy Phys. 04 (2016) 048.
[46] A. Cordero-Cid, J. Hernandez-Sanchez, V. Keus, S. F. King, S. Moretti, D. Rojas, and D. Sokolowska, J. High Energy Phys. 12 (2016) 014.
[47] A. Cordero-Cid, J. Hernandez-Sanchez, V. Keus, S. Moretti, D. Rojas, and D. Sokolowska, Eur. Phys. J. C **80**, 135 (2020).
[48] A. Cordero-Cid, J. Hernandez-Sanchez, V. Keus, S. Moretti, D. Rojas-Ciofalo, and D. Sokolowska, Phys. Rev. D **101**, 095023 (2020).
[49] S. L. Glashow and S. Weinberg, Phys. Rev. D **15**, 1958 (1977); E. A. Paschos, Phys. Rev. D **15**, 1966 (1977).
[50] J. L. Hewett, arXiv:hep-ph/9406302.
[51] A. G. Akeroyd, S. Moretti, K. Yagyu, and E. Yildirim, Int. J. Mod. Phys. A **32**, 1750145 (2017).
[52] K. Kiers, A. Soni, and G. H. Wu, Phys. Rev. D **62**, 116004 (2000).
[53] M. Jung, A. Pich, and P. Tuzon, Phys. Rev. D **83**, 074011 (2011).
[54] M. Jung, X. Q. Li, and A. Pich, J. High Energy Phys. 10 (2012) 063.
[55] A. G. Akeroyd, S. Moretti, and M. Song, Phys. Rev. D **98**, 115024 (2018).
[56] H. E. Logan, S. Moretti, D. Rojas-Ciofalo, and M. Song, arXiv:2012.08846.
[57] S. Kanemura, M. Kubota, and K. Yagyu, J. High Energy Phys. 08 (2020) 026.